Nanoscale

PAPER

View Article Online
View Journal | View Issue

Cite this: *Nanoscale*, 2023, **15**, 4334

Thermal degradation of the bulk and interfacial traps at 85 °C in perovskite photovoltaics†

Alan Jiwan Yun, [a] Seokjoo Ryu, [a] Jiheon Lim, [a] Jinhyun Kim [b] and Byungwoo Park *[a]

Received 26th November 2022,
Accepted 25th January 2023

DOI: 10.1039/d2nr06608d

rsc.li/nanoscale

The facile formation of defects in halide perovskite has recently been regarded as the main bottleneck for both the efficiency and stability of perovskite solar cells (PSCs). Therefore, understanding and controlling defects and traps in PSCs is essential to achieving stable devices. Herein, the thermal degradation of perovskite solar cells at 85 °C is studied in terms of electronic traps and device performance, of which the correlations are discussed. In particular, the shifts and changes in both energetic and spatial distributions of electronic defects are observed by capacitance plus impedance analyses under thermal stress. As the energy level and density of deep traps are quantitatively investigated, both the relaxation and degradation of the traps are identified at different timescales. Additionally, the trap densities are individually traced by positions during thermal degradation, where distinct evolutions are visualized. Notably, the traps are measured dominant at the interface between the perovskite and electron-transport layer (ETL). However, LiF incorporation mitigates the electronic traps by an order of magnitude at both interfaces throughout the thermal degradation, indicating that LiF incorporation reduces the initial trap density and suppresses the further formation of traps near the interfaces.

1. Introduction

Despite descent performance and cost efficiency as photovoltaic materials, organometal halide perovskite currently inheres a limitation in terms of the easy formation of defects owing to its solution-processed fabrication.[1–9] Although various defects and traps are expected in terms of their origins and energy/depth positions, they are commonly accused of causing anomalous phenomena by hindering the generation and transport of photocarriers in PSCs.[7,9–20] Moreover, these defects are reported as the prime origin that deteriorates the long-term stability of PSCs under practical conditions, *i.e.* 1 sun illumination and/or 85 °C temperature.[21] Owing to the low activation energy of ion migration, the defects in the perovskite not only cause microscopic degradation of materials, such as phase transition and decomposition, but also affect carrier dynamics and energy levels at the interfaces.[18,22–25]

Therefore, controlling the defects either in the bulk or at the interfaces has recently been considered alpha and omega for commercializing PSCs. Various strategies have been ardently reported to passivate the traps and defects of polycrystalline perovskite with great improvements in stability against air, light, and heat.[26–35] For example, Jeong *et al.* modified perovskite with pseudo-halide anion formate ($HCOO^-$) to control the anion vacancies at the grain boundaries and surfaces of the film.[36] Li *et al.* doped alkali fluorides into the perovskite and achieved 1000 h stability at 85 °C retaining over 80% of the initial efficiency with the spiro-OMeTAD-based hole-transport layer (HTL), confirming that the degradation of PSC depends more on perovskite defects than on the electrode materials.[37] Several recent tactics utilize additional ionic species into the perovskite without noticeable modification of its macroscopic properties, which leaves the insight that adjusting a morsel of defects is what significantly matters in forbidding the degradation of PSCs.[22,36–42] Hence, studying the degradation of nanoscale defects is becoming increasingly important during the degradation of PSC, and systematic investigations on electronic trap properties must be conducted to achieve efficient and stable photovoltaic materials/devices.[43–46]

In this study, the thermal degradation of PSCs is scrutinized in three aspects: photovoltaic performance, trap density of states (tDOS), and depth-profile trap density. The measurements were conducted for two-type solar cells, reference and

[a]*Department of Materials Science and Engineering, Research Institute of Advanced Materials, Seoul National University, Seoul 08826, Korea.*
E-mail: byungwoo@snu.ac.kr; Fax: +82-2-885-9671; Tel: +82-2-880-8319
[b]*Department of Chemical and Materials Engineering, The University of Suwon, Hwaseong 18323, Korea*

† Electronic supplementary information (ESI) available: Extended measurements on the devices for the incident photon-to-electron conversion efficiency, SIMS data, schematics and additional data for the impedance and capacitance analyses. See DOI: https://doi.org/10.1039/d2nr06608d

metal–fluoride modified, before and after 85 °C stored over 20, 50, 120, 250, 400, 600, and 1000 h. By adopting both impedance and drive-level capacitance profiling (DLCP) analyses, the energetic and spatial distributions of the electronic traps in PSC devices are examined. Shifts and evolution of the traps are quantitatively observed in terms of energy level and spatial position as thermal degradation occurs, and their mechanisms and correlations with the photovoltaic parameters are discussed in this study.

2. Results and discussion

To investigate the temporal evolution of three aspects of PSCs, solar cells were prepared by fabricating two types of active materials: bare $Cs_{0.05}(FA_{0.83}MA_{0.17})_{0.95}Pb(I_{0.83}Br_{0.17})_3$ (CsFAMA) and LiF-doped CsFAMA (CsFAMA:LiF) (Fig. 1(a)). With the triple-cation perovskite (quite stable at 85 °C), it is expected that the changes in nanoscale trap properties essentially determine the overall degradation of solar cells, while the micro-/macro-scale material degradation is insignificant.[47–50] Additionally, to avoid the degradation of electrodes being a determining factor for device stability, thermally stable PTAA was adopted as a hole-transporting material instead of spiro-OMeTAD.[45] The incorporation of alkali fluorides has been reported to effectively improve the long-term stability of PSCs by controlling the defects/traps in the bulk and at the grain boundaries/interfaces.[30,37,45] In particular, the LiF-incorporated perovskite does not exhibit a significant transformation in morphology or crystal phase at 85 °C.[30,45] The performances of both CsFAMA and CsFAMA:LiF are compared in Fig. 1(b), showing slight increases in short-circuit current density (J_{SC}), open-circuit voltage (V_{OC}), and fill factor (FF), while the *J–V* hysteresis effect decreases in CsFAMA:LiF. The improved photovoltaic process in CsFAMA:LiF is also certified by its enhanced quantum efficiency and steady-state current, as shown in Fig. S1.† Moreover, after 1500 h of storage at 85 °C, the CsFAMA:LiF device retains up to 91% of its initial PCE, with the bare CsFAMA showing 81% retention (Fig. 1(c)). Notably, the presence of LiF successfully restrains the thermal degradation of solar cells, and further measurements and analyses were conducted on the devices during the thermal stability tests to significantly understand the degradation mechanisms of PSCs with/without LiF.

First, the change in each photovoltaic parameter was traced as a function of the post-annealing time at 85 °C. The parameters demonstrated in Fig. 2(a–e) are extracted from the *J–V* characteristics of more than 10 devices each for CsFAMA and CsFAMA:LiF to certify that the results are reproducible. As shown in Fig. 2(a–e), V_{OC}, J_{SC}, PCE (= η), and FF exhibit better retention in CsFAMA:LiF than in CsFAMA. (Note that the PCE retention in Fig. 1(c) is better than that in Fig. 2(c), which is attributed to the different exposures to air during each measurement.) However, the *J–V* hysteresis index (HI ≡ ($\eta_{rev} - \eta_{for}$)/η_{rev}) decreases at the early stage, but soars after ~250 h, indicating down and up behaviors in the population of mobile ionic defects.[9–11,16,30,51] Interestingly, quite high HI is measured in CsFAMA after 1000 h, while that of CsFAMA:LiF remains low, which implies that LiF notably suppresses the heat-induced formation of mobile defects. In Fig. 2(f) for CsFAMA, the formation of PbI_2 is observed mostly near the ETL through cross-sectional SEM after 1000 h at 85 °C, while it is barely visible in CsFAMA:LiF. This is somewhat consistent with the previous report on the formation of PbI_2 at 85 °C, where the growth of PbI_2 impurities was suppressed by the LiF incorporation, observed by the plane-view SEM and XRD.[30,45] However, no significant differences were identified by the cross-sectional SEM in the scale of hundreds of nanometers in this study.

To ensure that the stability variations originate from the redistribution of ions *via* migration, interdiffusion, *etc.*, the elemental depth profiling in the solar cell (Fig. S2†) was investigated before/after 85 °C annealing by secondary ion mass spectroscopy (SIMS). No significant changes in the distribution of constituents were observed after 250 h, and the additional Li^+ and F^- ions in the CsFAMA:LiF were majorly identified near the interfaces between the perovskite and charge-transport layers. Considering that the solar-cell performance strongly depends on the trap states at the interfaces, differences in the stabilities of the parameters (Fig. 2(a–e)) are

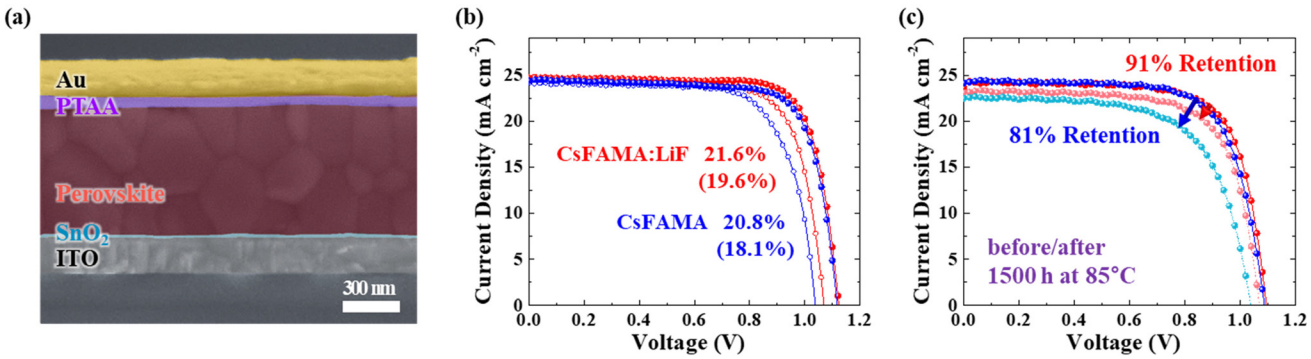

Fig. 1 Modification of the perovskite solar cell by LiF incorporation. (a) The architecture and dimension of the solar cell by SEM: ITO/SnO_2/perovskite/PTAA/Au. (b) The *J–V* curves of the champion devices with reverse scan (solid) and forward scan (open) and (c) the stability of the solar cells stored at 85 °C in N_2 for 1500 h, with (red) and without (blue) LiF.

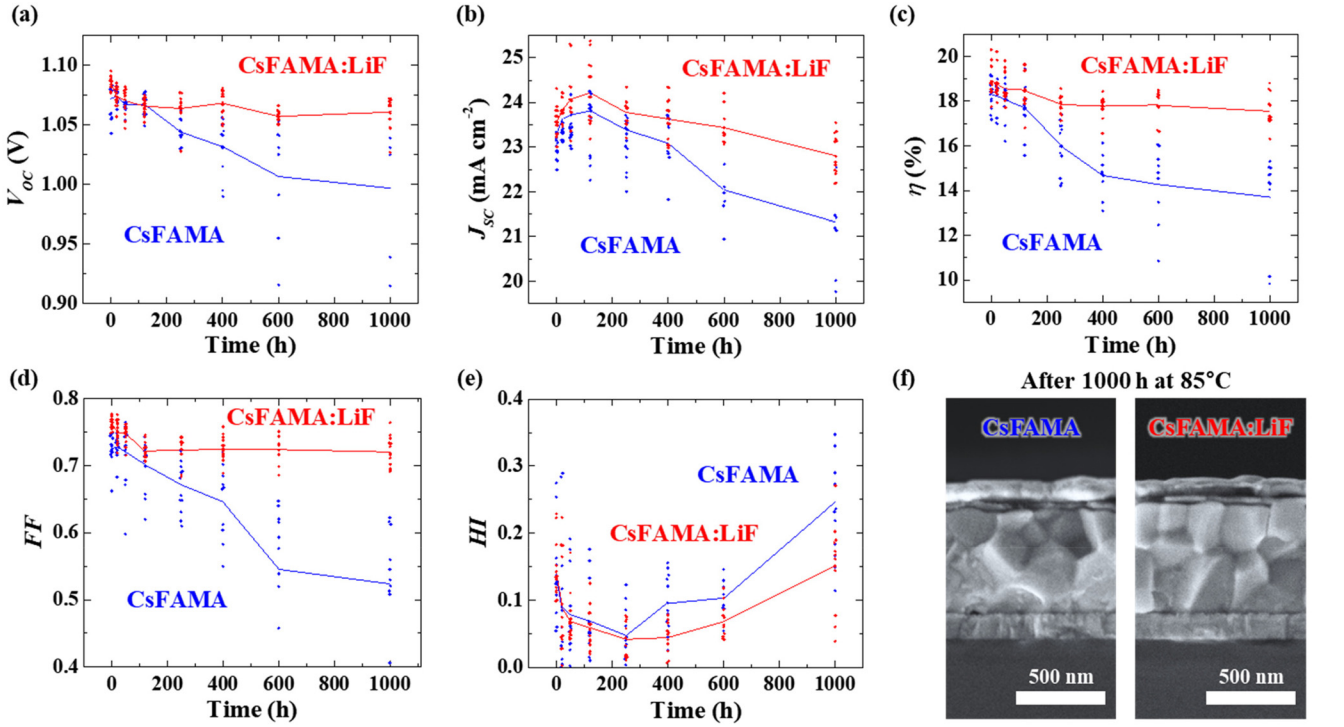

Fig. 2 Thermal stability of the photovoltaic parameters. (a) The open-circuit voltage (V_{OC}), (b) short-circuit current (J_{SC}), (c) power-conversion efficiency (η), (d) fill factor (FF), and (e) hysteresis index (HI) of the perovskite solar cells with/without LiF, as a function of post-annealing time at 85 °C. (f) Cross-sectional SEM images of the devices after 1000 h of the thermal test.

expected to be closely related to the trap formation and passivation near the interfaces without/with LiF.[37,40,52–57]

To investigate the transformations of trap properties underneath the degradation of solar-cell performance, the impedance $Z(\omega)$ of the device is explicitly measured (Fig. S3†). Comparing the Nyquist plots of the PSCs without/with LiF as a function of the post-annealing time, it is noted that the radius of the second semicircle in the CsFAMA:LiF device remains stable even after 1000 h of heating. The second-semicircle radius indicates the recombination resistance of the carriers in the perovskite, where its decrease in the CsFAMA device implies the additional formation of electronically active defects.[58] Furthermore, as previously reported, the derivative of capacitance ($C^Z \equiv [1/i\omega Z(\omega)]_{real}$) with respect to the AC frequency delivers essential information about the trap density of states [tDOS $N_t^Z(\omega)$] in a diode[37,52–54,59,60] (Fig. S4†). By adopting impedance analysis, the energy levels E_ω (with respect to the bandedge) and densities of deep/shallow traps are monitored as thermal degradation occurs, and these energetic trap-distribution spectra are demonstrated in Fig. 3(a). Even before the post annealing at 85 °C, the trap density in the deep-trap region ($E_\omega > 0.4$ eV) is almost half lower in CsFAMA:LiF than in CsFAMA (green symbols (0 h)). This certifies that LiF alloying successfully passivates the defects in solar-cell devices.

As thermal degradation proceeds, the trap density of states in both PSCs gradually shifts toward the bandedge with decreasing trap density in the deep-trap region (from green (0 h) to yellow (250 h)), which can be beneficial in terms of photovoltaic performance.[52,53,61,62] These favorable shifts of trap level and density, or the relaxations of traps, occur more immediately and drastically in CsFAMA:LiF. However, after a few hundreds of hours, the changes in trap level and density start to revert to the opposite direction with the increasing trap density and shift away from the bandedge (from yellow (250 h) to red (1000 h)). However, at 1000 h, the trap density of states ends notably shallow and reduces in CsFAMA:LiF more than in CsFAMA.

The phenomena observed by impedance spectroscopy for the evolution of tDOS $N_t^Z(\omega)$ during 1000 h are verified by fitting the trap levels and densities from ~20 individual devices (Fig. 3(b) and S5†). Two distinct evolutions are identified: the heat-induced relaxation of the traps (shift toward the bandedge and decreasing density) at the early stage from 0 to ~250 h, and the heat-induced degradation of the traps (shift away from the bandedge and increasing density) at the late stage from ~250 to 1000 h at 85 °C. This behavior of the trap properties somewhat resembles those of J_{SC} and HI illustrated in Fig. 2, where the enhancement at the early stage is followed by the gradual deterioration after ~200 h.

The relaxation of the electronic traps at the early stage of post annealing is more likely to be induced by local changes in chemical bonds among the atoms near the interfaces[25,42,57,58,63] instead of ionic redistributions within the solar cell (Fig. S2†). With this viewpoint, the accelerated relaxation in CsFAMA:LiF suggests that excessive F^- and Li^+ ions at the interfaces may boost the elimination of interfacial defects

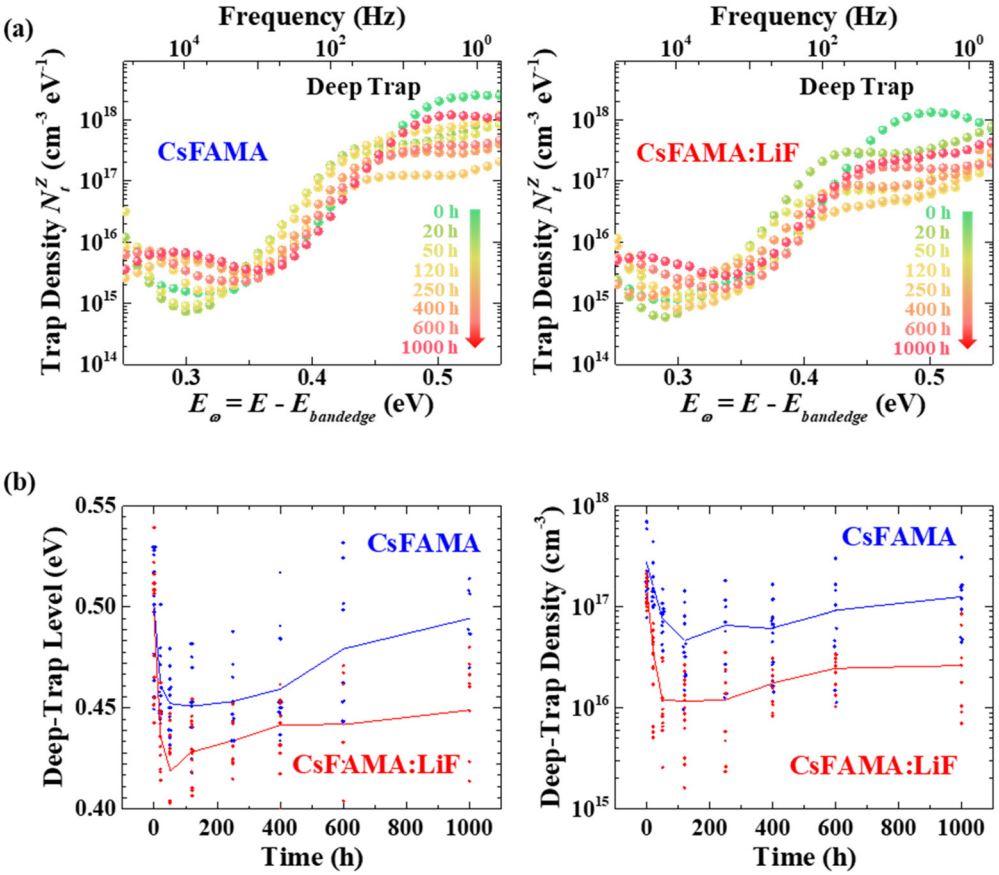

Fig. 3 Evolution of the electronic traps $N_t^Z(\omega)$ analyzed by impedance spectroscopy. (a) The spectra of the trap density of states [tDOS $N_t^Z(\omega)$] without and with LiF incorporation, aged under thermal stress at 85 °C. (b) The evolution of the deep-trap levels and integrated trap densities of PSCs, measured for ~20 devices.

at 85 °C, possibly by occupying the residual vacancies and/or passivating the dangling bonds, which are commonly reported behaviors of alkali–metal cations and fluoride anions.[31,37,39] Moreover, the degradation of traps from ~250 to 1000 h is greatly suppressed by LiF (Fig. 3(b)). It should be noted that LiF forbids the additional formation of traps under thermal stress, but the underlying mechanisms must be further clarified.

As discussed above, the trap density of states in PSC showed complicated evolutions at 85 °C, and deeper investigation of the traps is needed with consideration of their origins and positions. Therefore, drive-level capacitance profiling (DLCP) was adopted to observe how traps evolve in terms of spatial position during thermal degradation. The DLCP analysis measures the capacitance of the device as a function of both DC bias and AC perturbation at a given frequency, and it allows derivation in the carrier concentrations as a function of spatial depth (Fig. S4†).[6,18,64,65] The band diagrams based on the parameters of the solar cells utilized in this study are demonstrated in Fig. S6,†[54,62,66–68] which schematically explains the significance of DC bias in the depth-profile trap analysis.

The depth-profile trap distributions obtained by the DLCP analysis [DLCP $N_t^C(x,\omega)$] are demonstrated in Fig. 4(a), which exhibits clear U-shaped spectra. It is assumed that the measured concentration at high AC frequency ($f \cong 1$ MHz) contains only the free carriers in the device, and the trap density [$N_t^C(x,\omega)$] at low frequencies ($f \leq 100$ kHz or $E_\omega \geq 0.25$ eV) is estimated by subtracting the free carrier density from the total carrier concentration [$N_t^C(x,\omega) = N^C(x,\omega) - N_0^C(x,_{MHz})$] (Fig. S4†).[6] As thermal degradation proceeds, the bulk trap density consistently increases in both CsFAMA and CsFAMA:LiF. However, the evolutions of trap density at the interfaces include the ambiguity of growth and/or decay, depending on which sides the interfaces are at. To certify that the observation in Fig. 4(a) is the general case, ~10 devices for each type are analyzed and better monitored by mapping the spatial-distribution spectra in Fig. 4(b). Interestingly, as the devices are thermally degraded, the growth of the traps at the positions close to the interfaces ($\langle x \rangle \cong 75$ and 525 nm) is largely restrained in CsFAMA:LiF apparently owing to the LiF alloying. Consequently, the U-shape of trap distribution appears high and narrow in CsFAMA after degradation at 85 °C, while a relatively low and wide U-shape is identified in CsFAMA:LiF (Fig. S7†). It can be suggested that thinner layers of trap-rich regions are formed near the interfaces in CsFAMA:LiF, which could be responsible for its better charge-transfer functions through the interfaces from 85 °C stress.

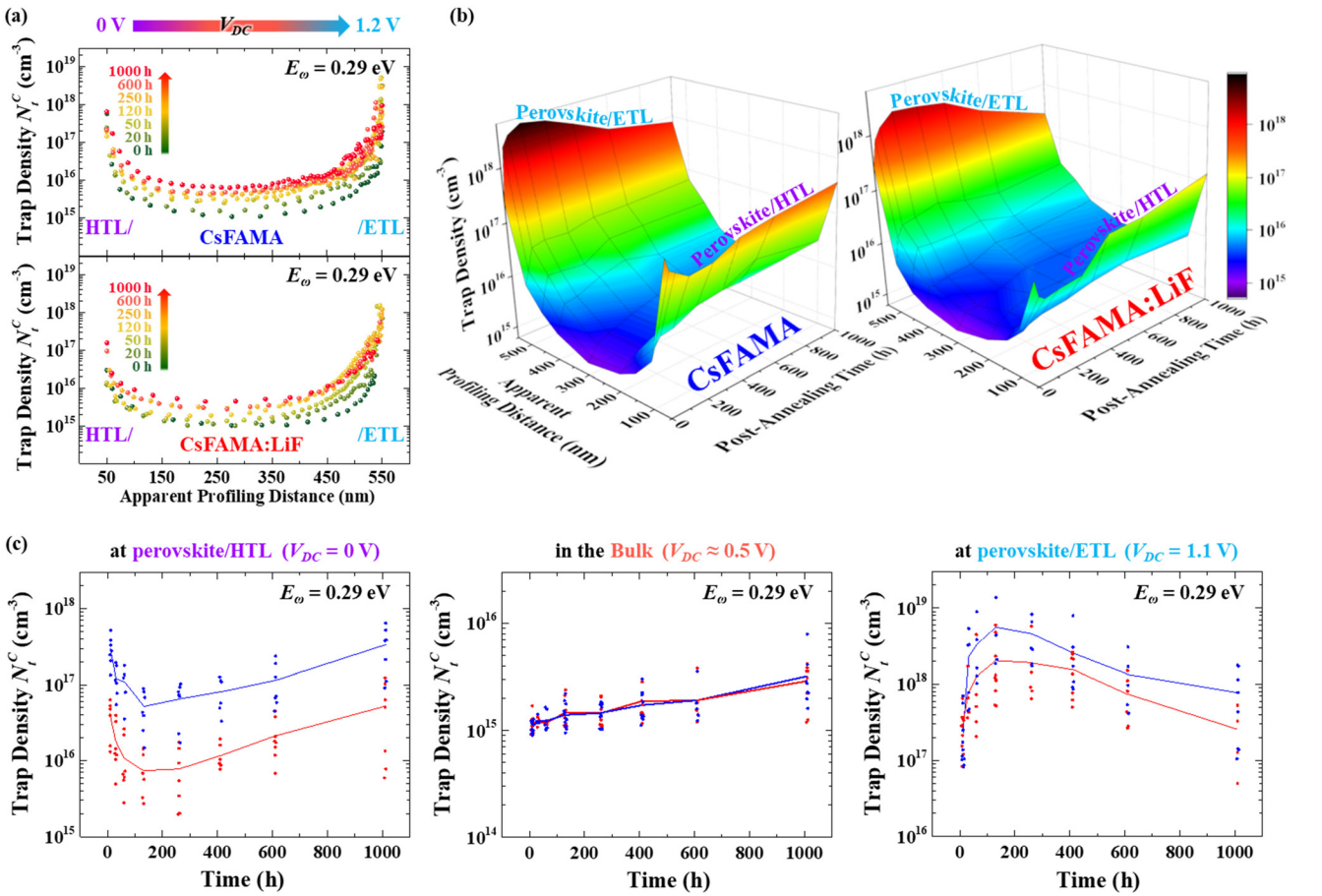

Fig. 4 Evolution in the spatial distribution of the electronic traps $N_t^C(x,\omega)$ analyzed by drive-level capacitance profiling. (a) Depth-profile trap density of the solar cells measured by the drive-level capacitance profiling analysis [DLCP $N_t^C(x,\omega)$] at 20 kHz, and (b) mapping of the trap distribution as a function of time during the thermal stability test at 85 °C. (c) The statistics of the trap densities measured at V_{DC} of 0, ~0.5, and 1.1 V. Data were collected from ~10 devices for CsFAMA and CsFAMA:LiF.

The statistical evolutions of the trap density at three representative positions (perovskite/HTL interface, bulk, and perovskite/ETL interface (Fig. S6†)) are individually traced, as depicted in Fig. 4(c) and S8.†[6,18,69] The gradual decrease in $N_t^C(x,\omega)$ at the perovskite/ETL interface after 250 h may be attributed to the redistribution of traps, *i.e.* the migration of defects toward the perovskite/HTL interface. Additionally, the trap densities at perovskite/ETL are measured to be an order of magnitude higher than those at perovskite/HTL, which certifies that the defects at the perovskite/ETL interface are more dominant in quantity and their impacts on the stability of n–i–p PSC (Fig. 2(f)). However, the evolutions of trap densities $N_t^C(x,\omega)$ at the ETL and HTL interfaces show an opposite trend, which needs to be further explored. The DLCP analyses are also performed at various frequencies (E_ω = 0.25, 0.32 and 0.36 eV (Fig. S8†)), and the evolutions of electronic traps at the given positions exhibit similar trends, as demonstrated in Fig. 4c (E_ω = 0.29 eV).

The traps at the perovskite/HTL and perovskite/ETL interfaces are almost an order of magnitude lower in CsFAMA:LiF than in CsFAMA throughout 1000 h of post-annealing (Fig. 4(c)). This confirms that LiF suppresses initial defect formation during the fabrication process, plays a role in healing residual defects, mitigates further degradation, and immobilizes additional defects at 85 °C. Moreover, the growths of the bulk trap densities do not show significant differences between CsFAMA:LiF and CsFAMA. The effects of the LiF incorporation are more confined at the interfaces, and the performance of photovoltaics mainly depends on the traps at the interfaces, where the densities of traps differ by orders of magnitude, rather than in the bulk.

The temporal analyses of the impedance and capacitance deliver a pile of unraveled information concerned with the 85 °C thermal degradation of PSCs. As discussed above, the transitions in the trap density of states and depth-profile trap distribution are observed, and their behaviors under thermal stress provide insights for effective strategies to control complex defects and traps. In addition, changes in some photovoltaic parameters are not fully explained by the evolution of the trap properties (from tDOS and DLCP) because the device performance is determined by the mixture of various factors in materials and interfaces simultaneously.

Moreover, the extended scientific messages are somewhat undisclosed under the possible measurement perturbation, which is currently a limitation of DLCP analysis methods for nanoscale trap properties. The observation of interesting phenomena in this study is expected to offer an important footstep for further studies on the evolution and degradation of electronic traps, which is key to further resolving the stability issues of hybrid perovskite-based photovoltaics.

3. Conclusions

The thermal degradations of CsFAMA and CsFAMA:LiF at 85 °C were systematically monitored for 1000 h in three individual aspects: photovoltaic performance, trap density of states, and depth-profile trap density. By performing impedance and DLCP analyses, the evolutions of the electronic traps are investigated in terms of energy level and depth position as a function of the post-annealing time. The heat-induced relaxation and degradation of traps are observed in this study, and the role of LiF in the middle of these phenomena is surmised. By tracing the shifts and changes in the trap distributions, F^- and Li^+ ions are found to be involved in curing and immobilizing defects at the interfaces, where the defects tend to proliferate and shift toward the bulk. Although revealing the exact origins of the measured traps is still challenging owing to the absence of accurate analysis methods for the electronic defects in 3D nanoscales, the observed trap evolutions in both energetic and depth aspects offer an important step to unravel the underlying science beneath the degradation of perovskite solar cells.

4. Experimental section

Solar cell fabrication

The patterned ITO substrate (AMG) was cleaned by sonication in acetone, isopropyl alcohol, and deionized water for 20 min each. The substrates were treated with a UV-ozone cleaner (UVC-150, Omniscience) for 15 min. For the electron-transport layer (ETL), diluted SnO_2 nanoparticles in H_2O (Alfa-Aesar) were prepared with the addition of tetramethylammonium hydroxide (TMAH, Sigma-Aldrich) by 7.5 vol%. The SnO_2 ETL was deposited on the substrate by spin-coating the SnO_2 nanoparticles at 3000 rpm for 30 s and dried at 120 °C for 30 min on a hot plate. The surface of the 30 nm-thick SnO_2 nanoparticle layer was UV-ozone treated for 15 min.

0.065 M of cesium iodide (CsI, TCI Chemicals), 1.00 M of formamidinium iodide (FAI, Great Solar Laboratory), 0.20 M of methylammonium bromide (MABr, Great Solar Laboratory), 1.1 M of lead iodide (PbI_2, TCI Chemicals), and 0.2 M of lead bromide ($PbBr_2$, TCI Chemicals) were dissolved in a mixture of *n*,*n*-dimethylformamide (DMF, Sigma-Aldrich) and dimethylsulfoxide (DMSO, Sigma-Aldrich) (volume ratio of 4 : 1). For CsFAMA:LiF, 2.4 mM of LiF was added to the precursor solution. For the perovskite active layer, the precursor solutions were spin-coated on the ITO/SnO_2 substrates with the spinning program: (1) 1000 rpm for 10 s and (2) 5000 rpm for 20 s sequentially. Anhydrous chlorobenzene (Sigma-Aldrich) was used as an antisolvent, 200 μL of which was dropped 5 s before the spinning program ended. The as-fabricated perovskite films were annealed at 100 °C on a hot plate for 30 min. For the polymer-based hole-transport layer (HTL), 17.5 mg of PTAA (33 kDa, MS Solutions) was dissolved in 1 mL of chlorobenzene (Sigma-Aldrich), and 6 μL of 4-*tert*-butylpyridine (tBP, Sigma-Aldrich) and 4 μL of bis(trifluoromethane)sulfonimide lithium salt (Li-TFSI, Sigma-Aldrich) solution (520 mg mL^{-1} in acetonitrile) were added as dopants. The PTAA solution was deposited on the substrate by spin-coating at 3000 rpm for 30 s. Au was thermally evaporated onto the device, with the desired thickness of ~80 nm.

Characterization

Thermal stability was tested using a thermostat in an N_2-filled glove box. The devices stored at 85 °C in N_2 were cooled at room temperature for more than 2 h before the measurements and analyses. The voltage dependence of photocurrent density (*J*–*V*) and steady-state current density was measured using a potentiostat (CHI 604A, CH Instrument) under 1 sun illumination from a solar simulator (K-3000, McScience). A mask with an aperture of 0.09 cm^2 was utilized to control the active area during the *J*–*V* characterization. The voltage was swept in the reverse/forward directions from 1.2 to −0.1 V and *vice versa*, both at a rate of 100 mV s^{-1}. The solar simulator was calibrated for every measurement, and the solar cells were stabilized under AM 1.5 G for at least 1 min. The external quantum efficiency of the solar cell was measured using an incident photon-to-current efficiency measurement system (QEX7, CEXCI). The cross-sectional images of the perovskite solar cells were observed using a field-emission scanning electron microscope (Merlin Compact: Zeiss). For the depth profiling of elemental distribution, a time-of-flight secondary ion mass spectrometer (TOF-SIMS : ION-TOF) was utilized, Bi was used as a primary source, and Cs and oxygen were used as etching sources. Areas of the analysis and etching were 100 × 100 μm^2 and 500 × 500 μm^2, respectively. For the analysis of the trap density of states, the impedance of the device was measured using a potentiostat (Zive SP-1: WonATech), with AC perturbation of 20 mV amplitude and frequency ranging from 10^{-2} to 10^6 Hz. The impedance analysis was performed under short-circuit conditions without DC bias or illumination. Before the measurement, the samples were rested in the dark until the internal voltage dropped below 3 mV. Drive-level capacitance profiling (DLCP) was performed using an LCR meter (E4980A: Keysight). The capacitance of the solar cells was measured with varying DC and AC voltages from 0 to 1.1 V and from 5 to 60 mV, respectively. Each cycle was performed at frequencies of 1, 5, 20, and 100 kHz.

Author contributions

A. J. Y. and B. P. conceived and conceptualized this study. A. J. Y. planned and performed the experiments, and carried out the measurements and data analyses. S. R. helped the capacitance measurement and data analysis. J. L. helped the fabrication of the solar cells. J. K. and B. P. provided insights to write the manuscript. A. J. Y. and B. P. jointly wrote the manuscript. S. R., J. L., and J. K. helped correction of the manuscript. All authors discussed the results and contributed to the final manuscript.

Conflicts of interest

The authors declare no conflict of interest.

Acknowledgements

This work is funded by the National Research Foundation of Korea (NRF, 2020R1A2C100545211), and by the Korea Institute of Energy Technology Evaluation and Planning (KETEP, 20183010014470). Research Institute of Advanced Materials (RIAM) and National Center for Inter-university Research Facilities (NCIRF) at Seoul National University are acknowledged for the technical supports in material investigations.

References

1 D. Meggiolaro, E. Mosconi and F. De Angelis, Formation of Surface Defects Dominates Ion Migration in Lead-Halide Perovskites, *ACS Energy Lett.*, 2019, **4**, 779–785.
2 X. Zhang, M. E. Turiansky, J.-X. Shen and C. G. Van de Walle, Iodine Interstitials as a Cause of Nonradiative Recombination in Hybrid Perovskites, *Phys. Rev. B*, 2020, **101**, 140101.
3 S. Reichert, J. Flemming, Q. An, Y. Vaynzof, J.-F. Pietschmann and C. Deibel, Ionic-Defect Distribution Revealed by Improved Evaluation of Deep-Level Transient Spectroscopy on Perovskite Solar Cells, *Phys. Rev. Appl.*, 2020, **13**, 034018.
4 J. Xing, Q. Wang, Q. Dong, Y. Yuan, Y. Fang and J. Huang, Ultrafast Ion Migration in Hybrid Perovskite Polycrystalline Thin Films under Light and Suppression in Single Crystals, *Phys. Chem. Chem. Phys.*, 2016, **18**, 30484–30490.
5 M. Ledinský, A. Vlk, T. Schönfeldová, J. Holovský, E. Aydin, H. X. Dang, Z. Hájková, L. Landová, J. Valenta, A. Fejfar and S. D. Wolf, Impact of Cation Multiplicity on Halide Perovskite Defect Densities and Solar Cell Voltages, *J. Phys. Chem. C*, 2020, **124**, 27333–27339.
6 Z. Ni, C. Bao, Y. Liu, Q. Jiang, W.-Q. Wu, S. Chen, X. Dai, B. Chen, B. Hartweg, Z. Yu, Z. Holman and J. Huang, Resolving Spatial and Energetic Distributions of Trap states in Metal Halide Perovskite Solar Cells, *Science*, 2020, **367**, 1352–1358.
7 G. Xing, N. Mathews, S. S. Lim, N. Yantara, X. Liu, D. Sabba, M. Grätzel, S. Mhaisalkar and T. C. Sum, Low-Temperature Solution-Processed Wavelength-Tunable Perovskites for Lasing, *Nat. Mater.*, 2014, **13**, 476–480.
8 W. Peng, B. Anand, L. Liu, S. Sampat, B. E. Bearden, A. V. Malko and Y. J. Chabal, Influence of Growth Temperature on Bulk and Surface Defects in Hybrid Lead Halide Perovskite Films, *Nanoscale*, 2016, **8**, 1627–1634.
9 T. Hwang, B. Lee, J. Kim, S. Lee, B. Gil, A. J. Yun and B. Park, From Nanostructural Evolution to Dynamic Interplay of Constituents: Perspectives for Perovskite Solar Cells, *Adv. Mater.*, 2018, **30**, 1704208.
10 D. A. Jacobs, Y. Wu, H. Shen, C. Barugkin, F. J. Beck, T. P. White, K. Weber and K. R. Catchpole, Hysteresis Phenomena in Perovskite Solar Cells: The Many and Varied Effects of Ionic Accumulation, *Phys. Chem. Chem. Phys.*, 2017, **19**, 3094–3103.
11 C. Li, S. Tscheuschner, F. Paulus, P. E. Hopkinson, J. Kießling, A. Köhler, Y. Vaynzof and S. Huettner, Iodine Migration and Its Effect on Hysteresis in Perovskite Solar Cells, *Adv. Mater.*, 2016, **28**, 2446–2454.
12 M. H. Futscher, J. M. Lee, L. McGovern, L. A. Muscarella, T. Wang, M. I. Haider, A. Fakharuddin, L. Schmidt-Mende and B. Ehrler, Quantification of Ion Migration in $CH_3NH_3PbI_3$ Perovskite Solar Cells by Transient Capacitance Measurements, *Mater. Horiz.*, 2019, **6**, 1497–1503.
13 A. Senocrate, I. Moudrakovski, G. Y. Kim, T.-Y. Yang, G. Gregori, M. Grätzel and J. Maier, The Nature of Ion Conduction in Methylammonium Lead Iodide: A Multimethod Approach, *Angew. Chem., Int. Ed.*, 2017, **56**, 7755–7759.
14 T. J. Jacobsson, J.-P. Correa-Baena, E. H. Anaraki, B. Philippe, S. D. Stranks, M. E. F. Bouduban, W. Tress, K. Schenk, J. Teuscher, J.-E. Moser, H. Rensmo and A. Hagfeldt, Unreacted PbI_2 as a Double-Edged Sword for Enhancing the Performance of Perovskite Solar Cells, *J. Am. Chem. Soc.*, 2016, **138**, 10331–10343.
15 C. Eames, J. M. Frost, P. R. F. Barnes, B. C. O'Regan, A. Walsh and M. S. Islam, Ionic Transport in Hybrid Lead Iodide Perovskite Solar Cells, *Nat. Commun.*, 2015, **6**, 7497.
16 Y. Chen, W. Zhou, X. Chen, X. Zhang, H. Gao, N. Aida, N. Ouedraogo, Z. Zheng, C. B. Han, Y. Zhang and H. Yan, In Situ Management of Ions Migration to Control Hysteresis Effect for Planar Heterojunction Perovskite Solar Cells, *Adv. Funct. Mater.*, 2022, **32**, 2108417.
17 K. Frohna, M. Anaya, S. Macpherson, J. Sung, T. A. S. Doherty, Y.-H. Chiang, A. J. Winchester, K. W. P. Orr, J. E. Parker, P. D. Quinn, K. M. Dani, A. Rao and S. D. Stranks, Nanoscale Chemical Heterogeneity Dominates the Optoelectronic Response of Alloyed Perovskite Solar Cells, *Nat. Nanotechnol.*, 2022, **17**, 190–196.
18 Z. Ni, H. Jiao, C. Fei, H. Gu, S. Xu, Z. Yu, G. Yang, Y. Deng, Q. Jiang, Y. Liu, Y. Yan and J. Huang, Evolution of defects during the degradation of metal halide perovskite solar cells under reverse bias and illumination, *Nat. Energy*, 2022, **7**, 65–73.

19 D. J. Slotcavage, H. I. Karunadasa and M. D. McGehee, Light-Induced Phase Segregation in Halide Perovskite Absorbers, *ACS Energy Lett.*, 2016, **1**, 1199–1205.

20 S. Reichert, Q. An, Y.-W. Woo, A. Walsh, Y. Vaynzof and C. Deibel, Probing the Ionic Defect Landscape in Halide Perovskite Solar Cells, *Nat. Commun.*, 2020, **11**, 6098.

21 M. V. Khenkin, E. A. Katz, A. Abate, G. Bardizza, J. J. Berry, C. Brabec, F. Brunetti, V. Bulović, Q. Burlingame, A. Di Carlo, R. Cheacharoen, Y.-B. Cheng, A. Colsmann, S. Cros, K. Domanski, M. Dusza, C. J. Fell, S. R. Forrest, Y. Galagan, D. Di Girolamo, M. Grätzel, A. Hagfeldt, E. von Hauff, H. Hoppe, J. Kettle, H. Köbler, M. S. Leite, S. F. Liu, Y.-L. Loo, J. M. Luther, C.-Q. Ma, M. Madsen, M. Manceau, M. Matheron, M. McGehee, R. Meitzner, M. K. Nazeeruddin, A. F. Nogueira, Ç. Odabaşı, A. Osherov, N.-G. Park, M. O. Reese, F. De Rossi, M. Saliba, U. S. Schubert, H. J. Snaith, S. D. Stranks, W. Tress, P. A. Troshin, V. Turkovic, S. Veenstra, I. Visoly-Fisher, A. Walsh, T. Watson, H. Xie, R. Yıldırım, S. M. Zakeeruddin, K. Zhu and M. Lira-Cantu, Consensus Statement for Stability Assessment and Reporting for Perovskite Photovoltaics Based on ISOS Procedures, *Nat. Energy*, 2020, **5**, 35–49.

22 F. Ye, H. Wang, W. Ke, C. Tao and G. Fang, Unveiling the Key Factor Affecting the Illumination Deterioration and Response Measures for Lead Halide Perovskite Solar Cells, *J. Energy Chem.*, 2022, **73**, 429–435.

23 K. Domanski, B. Roose, T. Matsui, M. Saliba, S.-H. Turren-Cruz, J.-P. Correa-Baena, C. R. Carmona, G. Richardson, J. M. Foster, F. De Angelis, J. M. Ball, A. Petrozza, N. Mine, M. K. Nazeeruddin, W. Tress, M. Grätzel, U. Steiner, A. Hagfeldt and A. Abate, Migration of Cations Induces Reversible Performance Losses over Day/Night Cycling in Perovskite Solar Cells, *Energy Environ. Sci.*, 2017, **10**, 604–613.

24 Y. Yuan and J. Huang, Ion Migration in Organometal Trihalide Perovskite and Its Impact on Photovoltaic Efficiency and Stability, *Acc. Chem. Res.*, 2016, **49**, 286–293.

25 Y. Lin, L. Shen, J. Dai, Y. Deng, Y. Wu, Y. Bai, X. Zheng, J. Wang, Y. Fang, H. Wei, W. Ma, X. C. Zeng, X. Zhan and J. Huang, π-Conjugated Lewis Base: Efficient Trap-Passivation and Charge-Extraction for Hybrid Perovskite Solar Cells, *Adv. Mater.*, 2017, **29**, 1604545.

26 D.-Y. Son, S.-G. Kim, J.-Y. Seo, S.-H. Lee, H. Shin, D. Lee and N.-G. Park, Universal Approach toward Hysteresis-Free Perovskite Solar Cell via Defect Engineering, *J. Am. Chem. Soc.*, 2018, **140**, 1358–1364.

27 J. Kim, A. J. Yun, B. Gil, Y. Lee and B. Park, Triamine–Based Aromatic Cation as a Novel Stabilizer for Efficient Perovskite Solar Cells, *Adv. Funct. Mater.*, 2019, **29**, 1905190.

28 J. Kim, T. Hwang, B. Lee, S. Lee, K. Park, H. H. Park and B. Park, An Aromatic Diamine Molecule as the *A*–Site Solute for Highly Durable and Efficient Perovskite Solar Cells, *Small Methods*, 2019, **3**, 1800361.

29 M. J. Jeong, K. M. Yeom, S. J. Kim, E. H. Jung and J. H. Noh, Spontaneous Interface Engineering for Dopant-Free Poly (3-Hexylthiophene) Perovskite Solar Cells with Efficiency over 24%, *Energy Environ. Sci.*, 2021, **14**, 2419–2428.

30 A. J. Yun, J. Kim, B. Gil, H. Woo, K. Park, J. Cho and B. Park, Incorporation of Lithium Fluoride Restraining Thermal Degradation and Photodegradation of Organometal Halide Perovskite Solar Cells, *ACS Appl. Mater. Interfaces*, 2020, **12**, 50418–50425.

31 H. Zeng, L. Li, F. Liu, M. Li, S. Zhang, X. Zheng, L. Luo, S. You, Y. Zhao, R. Guo, Z. Gong, R. Huang, Z. Li, T. Wang, Y. Cui, Y. Rong and X. Li, Improved Performance and Stability of Perovskite Solar Modules by Regulating Interfacial Ion Diffusion with Nonionic Cross-Linked 1D Lead-Iodide, *Adv. Energy Mater.*, 2022, **12**, 2102820.

32 J. Cao, S. X. Tao, P. A. Bobbert, C.-P. Wong and N. Zhao, Interstitial Occupancy by Extrinsic Alkali Cations in Perovskites and Its Impact on Ion Migration, *Adv. Mater.*, 2018, **30**, 1707350.

33 M. Stolterfoht, C. M. Wolff, J. A. Márquez, S. Zhang, C. J. Hages, D. Rothhardt, S. Albrecht, P. L. Burn, P. Meredith and D. Neher, Visualization and Suppression of Interfacial Recombination for High-Efficiency Large-Area *p-i-n* Perovskite Solar Cells, *Nat. Energy*, 2018, **3**, 847–854.

34 Q. Guo, F. Yuan, B. Zhang, S. Zhou, J. Zhang, Y. Bai, L. Fan, T. Hayat, A. Alsaedi and Z. Tan, Passivation of the Grain Boundaries of $CH_3NH_3PbI_3$ Using Carbon Quantum Dots for Highly Efficient Perovskite Solar Cells with Excellent Environmental Stability, *Nanoscale*, 2019, **11**, 115–124.

35 Z. Ma, R. Yu, Z. Xu, G. Wu, H. Gao, R. Wang, Y. Gong, J. Yang and Z. Tan, Crosslinkable and Chelatable Organic Ligand Enables Interfaces and Grains Collaborative Passivation for Efficient and Stable Perovskite Solar Cells, *Small*, 2022, **18**, 2201820.

36 J. Jeong, M. Kim, J. Seo, H. Lu, P. Ahlawat, A. Mishra, Y. Yang, M. A. Hope, F. T. Eickemeyer, M. Kim, Y. J. Yoon, I. W. Choi, B. P. Darwich, S. J. Choi, Y. Jo, J. H. Lee, B. Walker, S. M. Zakeeruddin, L. Emsley, U. Rothlisberger, A. Hagfeldt, D. S. Kim, M. Grätzel and J. Y. Kim, Pseudo-Halide Anion Engineering for α-$FAPbI_3$ Perovskite Solar Cells, *Nature*, 2021, **592**, 381–385.

37 N. Li, S. Tao, Y. Chen, X. Niu, C. K. Onwudinanti, C. Hu, Z. Qiu, Z. Xu, G. Zheng, L. Wang, Y. Zhang, L. Li, H. Liu, Y. Lun, J. Hong, X. Wang, Y. Liu, H. Xie, Y. Gao, Y. Bai, S. Yang, G. Brocks, Q. Chen and H. Zhou, Cation and Anion Immobilization through Chemical Bonding Enhancement with Fluorides for Stable Halide Perovskite Solar Cells, *Nat. Energy*, 2019, **4**, 408–415.

38 T. Matsui, T. Yamamoto, T. Nishihara, R. Morisawa, T. Yokoyama, T. Sekiguchi and T. Negami, Compositional Engineering for Thermally Stable, Highly Efficient Perovskite Solar Cells Exceeding 20% Power Conversion Efficiency with 85 °C/85% 1000 h Stability, *Adv. Mater.*, 2019, 1806823.

39 R. Azmi, N. Nurrosyid, S.-H. Lee, M. Al Mubarok, W. Lee, S. Hwang, W. Yin, T. K. Ahn, T.-W. Kim, D. Y. Ryu, Y. R. Do and S.-Y. Jang, Shallow and Deep Trap State Passivation for Low-Temperature Processed Perovskite Solar Cells, *ACS Energy Lett.*, 2020, **5**, 1396–1403.

40 X. Liu, Y. Zhang, L. Shi, Z. Liu, J. Huang, J. S. Yun, Y. Zeng, A. Pu, K. Sun, Z. Hameiri, J. A. Stride, J. Seidel, M. A. Green and X. Hao, Exploring Inorganic Binary Alkaline Halide to Passivate Defects in Low-Temperature-Processed Planar-Structure Hybrid Perovskite Solar Cells, *Adv. Energy Mater.*, 2018, **8**, 1800138.

41 B. Lee, T. Hwang, S. Lee, B. Shin and B. Park, Microstructural Evolution of Hybrid Perovskites Promoted by Chlorine and Its Impact on the Performance of Solar Cell, *Sci. Rep.*, 2019, **9**, 4803.

42 Y. Yang, L. Wu, X. Hao, Z. Tang, H. Lai, J. Zhang, W. Wang and L. Feng, Beneficial Effects of Potassium Iodide Incorporation on Grain Boundaries and Interfaces of Perovskite Solar Cells, *RSC Adv.*, 2019, **9**, 28561.

43 J. A. Christians, P. Schulz, J. S. Tinkham, T. H. Schloemer, S. P. Harvey, B. J. T. de Villers, A. Sellinger, J. J. Berry and J. M. Luther, Tailored Interfaces of Unencapsulated Perovskite Solar Cells for >1,000 Hour Operational Stability, *Nat. Energy*, 2018, **3**, 68–74.

44 J. Wu, J. Shi, Y. Li, H. Li, H. Wu, Y. Luo, D. Li and Q. Meng, Quantifying the Interface Defect for the Stability Origin of Perovskite Solar Cells, *Adv. Energy Mater.*, 2019, **9**, 1901352.

45 A. J. Yun, B. Gil, S. Ryu, J. Kim and B. Park, Evolution of the Electronic Traps in Perovskite Photovoltaics during 1000 h at 85 °C, *ACS Appl. Energy Mater.*, 2022, **5**, 7192–7198.

46 X. Zheng, X. Wang, W. Li, Z. Liu, W. Ming, H. Wang, H. Wang, D. Li, B. Liu and C. Yang, Correlations of Ionic Migration and Deep-Level Traps Leads to Surface Defect Formation in Perovskite Solar Cells, *J. Phys. Chem. C*, 2021, **125**, 19551–19559.

47 M. Saliba, T. Matsui, J.-Y. Seo, K. Domanski, J.-P. Correa-Baena, M. K. Nazeeruddin, S. M. Zakeeruddin, W. Tress, A. Abate, A. Hagfeldt and M. Grätzel, Cesium-Containing Triple Cation Perovskite Solar Cells: Improved Stability, Reproducibility and High Efficiency, *Energy Environ. Sci.*, 2016, **9**, 1989–1997.

48 O. A. Syzgantseva, M. Saliba, M. Grätzel and U. Rothlisberger, Stabilization of the Perovskite Phase of Formamidinium Lead Triiodide by Methylammonium, Cs, and/or Rb Doping, *J. Phys. Chem. Lett.*, 2017, **8**, 1191–1196.

49 N. J. Jeon, J. H. Noh, W. S. Yang, Y. C. Kim, S. Ryu, J. Seo and S. I. Seok, Compositional Engineering of Perovskite Materials for High-Performance Solar Cells, *Nature*, 2015, **517**, 476–480.

50 M. Saliba, T. Matsui, K. Domanski, J.-Y. Seo, A. Ummadisingu, S. M. Zakeeruddin, J.-P. Correa-Baena, W. R. Tress, A. Abate, A. Hagfeldt and M. Grätzel, Incorporation of Rubidium Cations into Perovskite Solar Cells Improves Photovoltaic Performance, *Science*, 2016, **354**, 206–209.

51 H. Snaith, A. Abate, J. M. Ball, G. E. Eperon, T. Leijtens, N. K. Noel, S. D. Stranks, J. T.-W. Wang, K. Wojciechowski and W. Zhang, Anomalous Hysteresis in Perovskite Solar Cells, *Phys. Chem. Lett.*, 2014, **5**, 1511–1515.

52 T. Hwang, A. J. Yun, J. Kim, D. Cho, S. Kim, S. Hong and B. Park, Electronic Traps and Their Correlations to Perovskite Solar Cell Performance via Compositional and Thermal Annealing Controls, *ACS Appl. Mater. Interfaces*, 2019, **11**, 6907–6917.

53 A. J. Yun, J. Kim, T. Hwang and B. Park, Origins of Efficient Perovskite Solar Cells with Low-Temperature Processed SnO_2 Electron Transport Layer, *ACS Appl. Energy Mater.*, 2019, **2**, 3554–3560.

54 L. Bertoluzzi, C. C. Boyd, N. Rolston, J. Xu, R. Prasanna, B. C. O'Regan and M. D. McGehee, Mobile Ion Concentration Measurement and Open-Access Band Diagram Simulation Platform for Halide Perovskite Solar Cells, *Joule*, 2020, **4**, 109–127.

55 H. Zhu, Y. Ren, L. Pan, O. Ouellette, F. T. Eickemeyer, Y. Wu, X. Li, S. Wang, H. Liu, X. Dong, S. M. Zakeeruddin, Y. Liu, A. Hagfeldt and M. Grätzel, Synergistic Effect of Fluorinated Passivator and Hole Transport Dopant Enables Stable Perovskite Solar Cells with an Efficiency Near 24%, *J. Am. Chem. Soc.*, 2021, **143**, 3231–3237.

56 Y. Dong, W. Shen, W. Dong, C. Bai, J. Zhao, Y. Zhou, F. Huang, Y.-B. Cheng and J. Zhong, Chlorobenzenesulfonic Potassium Salts as the Efficient Multifunctional Passivator for the Buried Interface in Regular Perovskite Solar Cells, *Adv. Energy Mater.*, 2022, 2200417.

57 B. Lee, S. Lee, D. Cho, J. Kim, T. Hwang, K. H. Kim, S. Hong, T. Moon and B. Park, Evaluating the Optoelectronic Quality of Hybrid Perovskites by Conductive Atomic Force Microscopy with Noise Spectroscopy, *ACS Appl. Mater. Interfaces*, 2016, **8**, 30985–30991.

58 J. Kim, Y. Lee, A. J. Yun, B. Gil and B. Park, Interfacial Modification and Defect Passivation by the Cross-Linking Interlayer for Efficient and Stable CuSCN-Based Perovskite Solar Cells, *ACS Appl. Mater. Interfaces*, 2019, **11**, 46818–46824.

59 Y. Shao, Z. Xiao, C. Bi, Y. Yuan and J. Huang, Origin and Elimination of Photocurrent Hysteresis by Fullerene Passivation in $CH_3NH_3PbI_3$ Planar Heterojunction Solar Cells, *Nat. Commun.*, 2014, **5**, 5784.

60 T. Walter, R. Herberholz, C. Müller and H. W. Schock, Determination of Defect Distributions from Admittance Measurements and Application to Cu(In,Ga)Se_2 Based Heterojunctions, *J. Appl. Phys.*, 1996, **80**, 4411–4420.

61 D. B. Khadka, Y. Shirai, M. Yanagida and K. Miyano, Degradation of Encapsulated Perovskite Solar Cells Driven by Deep Trap States and Interfacial Deterioration, *J. Mater. Chem. C*, 2018, **6**, 162–170.

62 D. Prochowicz, P. Yadav, M. Saliba, M. Saski, S. M. Zakeeruddin, J. Lewiński and M. Grätzel, Reduction in the Interfacial Trap Density of Mechanochemically Synthesized $MAPbI_3$, *ACS Appl. Mater. Interfaces*, 2017, **9**, 28418–28425.

63 A. R. M. Yusoff, M. Vasilopoulou, D. G. Georgiadou, L. C. Palilis, A. Abate and M. K. Nazeeruddin, Passivation and Process Engineering Approaches of Halide Perovskite Films for High Efficiency and Stability Perovskite Solar Cells, *Energy Environ. Sci.*, 2021, **14**, 2906–2953.
64 J. T. Heath, J. D. Cohen and W. N. Shafarman, Distinguishing Metastable Changes in Bulk CIGS Defect Densities from Interface Effects, *Thin Solid Films*, 2003, **431**, 426–430.
65 H.-S. Duan, W. Yang, B. Bob, C.-J. Hsu, B. Lei and Y. Yang, The Role of Sulfur in Solution-Processed $Cu_2ZnSn(S,Se)_4$ and Its Effect on Defect Properties, *Adv. Funct. Mater.*, 2012, **23**, 1466–1471.
66 U. Rau and T. Kirchartz, Charge Carrier Collection and Contact Selectivity in Solar Cells, *Adv. Mater. Interfaces*, 2019, **6**, 1900252.
67 I. Mora-Seró, How Do Perovskite Solar Cells Work?, *Joule*, 2018, **2**, 585–587.
68 M. Samiee, S. Konduri, B. Ganapathy, R. Kottokkaran, H. A. Abbas, A. Kitahara, P. Joshi, L. Zhang, M. Noack and V. Dalal, Defect Density and Dielectric Constant in Perovskite Solar Cells, *Appl. Phys. Lett.*, 2014, **105**, 153502.
69 O. Gunawan, S. R. Pae, D. M. Bishop, Y. Virgus, J. H. Noh, N. J. Jeon, Y. S. Lee, X. Shao, T. Todorov, D. B. Mitzi and B. Shin, Carrier-Resolved Photo-Hall Effect, *Nature*, 2019, **575**, 151–155.